

RELAXATION OF BLAZAR INDUCED PAIR BEAMS IN COSMIC VOIDS

FRANCESCO MINIATI

Physics Department, Wolfgang-Pauli-Strasse 27, ETH-Zürich, CH-8093, Zürich, Switzerland; fm@phys.ethz.ch

ANDRII ELYIV

Institut d'Astrophysique et de Géophysique, Université de Liège, 4000 Liège, Belgium and
Main Astronomical Observatory, Academy of Sciences of Ukraine, 27 Akademika Zabolotnoho St., 03680 Kyiv, Ukraine
Draft version March 9, 2022

ABSTRACT

The stability properties of a low density ultra relativistic pair beam produced in the intergalactic medium by multi-TeV gamma-ray photons from blazars are analyzed. The problem is relevant for probes of magnetic field in cosmic voids through gamma-ray observations. In addition, dissipation of such beams could affect considerably the thermal history of the intergalactic medium and structure formation. We use a Monte Carlo method to quantify the properties of the blazar induced electromagnetic shower, in particular the bulk Lorentz factor and the angular spread of the pair beam generated by the shower, as a function of distance from the blazar itself. We then use linear and non-linear kinetic theory to study the stability of the pair beam against the growth of electrostatic plasma waves, employing the Monte Carlo results for our quantitative estimates. We find that the fastest growing mode, like any perturbation mode with even a very modest component perpendicular to the beam direction, cannot be described in the reactive regime. Due to the effect of non-linear Landau damping, which suppresses the growth of plasma oscillations, the beam relaxation timescale is found significantly longer than the inverse Compton loss time. Finally, density inhomogeneities associated with cosmic structure induce loss of resonance between the beam particles and plasma oscillations, strongly inhibiting their growth. We conclude that relativistic pair beams produced by blazars in the intergalactic medium are stable on timescales long compared to the electromagnetic cascade's. There appears to be little or no effect of pair-beams on the intergalactic medium.

Subject headings: gamma rays: general – instabilities – intergalactic medium – plasmas – radiation mechanisms: non-thermal – relativistic processes

1. INTRODUCTION

Streaming relativistic particles are common in tenuous astrophysical plasma and their propagation and stability properties a recurrent theme. Examples include type III solar radio burst (Benz 1993), quasars' jets (Lesch & Schlickeiser 1987), cosmic-rays streaming out of star forming galaxies (Miniati & Bell 2011) and cosmic-ray transport in the intracluster medium (Ensslin et al. 2011). Propagation and stability properties, related in particular to the excitation of plasma waves, is subject of attentive investigation as they can play a crucial role in the interpretation of observational data.

Ultra-relativistic beams of e^+e^- pairs are also generated in the intergalactic medium (IGM) by very high energy gamma-rays from distant blazars, by way of photon-photon interactions with the extragalactic background light (EBL, Gould & Schröder 1967; Schlickeiser et al. 2012). While blazars' spectra, and in particular their multi-TeV cut-off features, have been studied in detail to constraint the EBL (e.g. Aharonian et al. 2006), recently multi-GeV and TeV blazars observations have also been used to constrain magnetic field in cosmic voids for the first time (Neronov & Vovk 2010; Tavecchio et al. 2010). In fact, for flat enough blazar's spectra, the electromagnetic cascade should produce an observable spectral bump at multi-GeV energies. The absence of such a bump in a number of observed blazars is as-

cribed to the presence of a sufficiently strong magnetic field, $B_v \gtrsim 10^{-16} \text{G}$, to deflect the pairs in less than an inverse Compton length, $l_{IC} \simeq \text{Mpc} (E_{\pm}/\text{TeV})^{-1} (1+z)^{-4}$, where z is the cosmological redshift (Plaga 1995; Neronov & Semikoz 2009). When time variability of the blazars is taken into account the above lower limit is relaxed to a more conservative value of $B_v \gtrsim 10^{-18} \text{G}$ (Dermer et al. 2011; Taylor et al. 2011). The required filling factor of the magnetic field is about 60% (Dolag et al. 2011). Other potential effects of a magnetic field in voids on the electromagnetic cascades have also been investigated, including extended emission around gamma-ray point-like sources (Aharonian et al. 1994; Neronov & Semikoz 2007; Dolag et al. 2009; Elyiv et al. 2009; Neronov et al. 2010a) and the delayed echoes of multi-TeV gamma-ray flares or gamma-ray bursts (Plaga 1995; Takahashi et al. 2008; Murase et al. 2008, 2009).

However, in principle the pair-beam is subject to various instabilities, in particular microscopic plasma instabilities of the two-stream family. On this account, Broderick et al. (2012) conclude that transverse modes of the two-stream instability act on much shorter timescales than inverse Compton scattering, effectively inhibiting the cascade and invalidating the above magnetic field measurements. In addition, as a result of the beam's relaxation, substantial amount of energy would be deposited into the IGM, with dramatic con-

sequences for its thermal history (Chang et al. 2012; Pfrommer et al. 2012).

In this paper, we reanalyze the stability of blazars induced ultra-relativistic pair beams. In particular, we use a Monte Carlo model of the electromagnetic shower to quantify the beam properties at various distances from the blazar, and analyze the stability of the produced beam following the work of Breizman, Rytov and collaborators (reviewed in Breizman & Rytov 1974; Breizman 1990). We find that even for very modest perpendicular components of the wave-vector, the analysis of the instability requires a kinetic treatment. We thus estimate the max growth rate of the instability and find that for bright blazars (with equivalent isotropic gamma-ray luminosity of 10^{45} erg s $^{-1}$) it is suppressed by Coulomb collisions at distances $D \gtrsim 50$ and 20 physical Mpc at redshift 0 and 3, respectively. Importantly, the growth rate of plasma oscillations is found to be severely suppressed by non-linear Landau damping, so that even at closer distances to the blazar the beam relaxation timescale remains considerably longer than the inverse Compton cooling time. Finally, the resonance condition cannot be maintained in the presence of density inhomogeneities associated to cosmological structure formation, which also act to dramatically suppress the instability. Thus our findings support the magnetic field based interpretation of the gamma-ray observational results and rule out effects of blazars' beam on the thermal history of the IGM. Broderick et al. did not consider the role of density inhomogeneities and concluded that non-linear Landau damping is unimportant, although they did not present a quantitative analysis of the process.

The rest of this paper is organized as follows. Sec. 2 summarizes the physical properties of pair beams produced by blazars and present the results of the Monte Carlo model. The two-stream instability in both the reactive and kinetic regimes is discussed in Sec. 3, where the max growth rate of the instability is also given and compared to the collisional rate. Nonlinear effects are considered in Sec. 4, where the timescales for the beam relaxation is derived. Finally, Sec. 5 briefly summarizes the results.

2. PAIR BEAMS IN VOIDS

In order to carry out the analysis of the stability of ultra-relativistic pair beams produced by blazars, we need to estimate characteristic quantities of the beam, including its density contrast to the IGM, the Lorentz factor, and angular and velocity spread. These quantities derive from the energy and number density of the pair producing photons, i.e. the blazar's spectral flux, F_γ , and the EBL model. Pair production has been studied extensively in the literature (e.g. Gould & Schröder 1967; Bonometto & Rees 1971; Schlickeiser et al. 2012) and in the following we briefly summarize its qualitative features, which we then use to describe the results of our Monte Carlo model of a blazar induced cascade.

2.1. Basic Qualitative Features

Pairs are most efficiently created just above the energy threshold for production, i.e. where

$$s \equiv E_\gamma E_{\text{EBL}}(1 - \cos \phi)/2m_e^2 c^4 \geq 1, \quad (1)$$

with ϕ the angle between the interacting photons, E_γ and E_{EBL} the energy of the incident and target EBL photon, respectively, and the relativistic invariant, s , the center of mass energy square in units $m_e^2 c^4$. The mean free path for the process depends on the details of the EBL model (Kneiske et al. 2004; Franceschini et al. 2008) but is approximately

$$\ell_{\gamma\gamma} \simeq 0.8 \left(\frac{E_\gamma}{\text{TeV}} \right)^{-1} (1+z)^{-\zeta} \text{Gpc}, \quad (2)$$

with $\zeta = 4.5$ for $z \leq 1$, $\zeta = 0$ otherwise (Neronov & Semikoz 2009; Broderick et al. 2012). The particle number density of the beam, n_b , is set by the balance of pair production rate, $2F_\gamma/\ell_{\gamma\gamma}$, evaluated close to production threshold, and energy loss rate. If inverse Compton losses dominate then, at a distance D from the blazar such that $F_\gamma = L_\gamma/4\pi D^2$,

$$n_b \simeq 2 \frac{F_\gamma}{c} \frac{\ell_{IC}}{\ell_{\gamma\gamma}} \simeq 3 \times 10^{-25} \text{cm}^{-3} \left(\frac{E_\gamma L_\gamma}{10^{45} \text{erg/s}} \right) \times \left(\frac{D}{\text{Gpc}} \right)^{-2} \left(\frac{E_\gamma}{\text{TeV}} \right) (1+z)^{\zeta-4}. \quad (3)$$

where, $E_\gamma L_\gamma$, is an estimate of the blazar's equivalent isotropic gamma-ray luminosity for a source at distance D (see, Broderick et al. 2012). Each pair particle carries about half the energy of the incident gamma-ray, so the beam Lorentz factor is

$$\Gamma = \frac{E_\gamma}{2m_e c^2} \sim 10^6 \left(\frac{E_\gamma}{\text{TeV}} \right). \quad (4)$$

Another important characteristic quantity of the beam is its angular spread, $\Delta\theta$, determined by the distribution of angles θ between the pair produced particles and the parent photons direction. This can be found to be related to Γ and the relativistic invariant as

$$\Delta\theta \leq \frac{s}{\Gamma} \left(1 - \frac{1}{s} \right)^{\frac{1}{2}}. \quad (5)$$

2.2. Monte Carlo Model

In this section we compute the characteristic quantities of a blazar induced pair beam, using a Monte Carlo model of the electromagnetic cascade, fully described in Elyiv et al. (2009) and applied also in Neronov et al. (2010). For the purpose, the blazar's spectral emission is a typical power law distribution of primary gamma-ray photons, $dn_\gamma/dE_\gamma \propto E_\gamma^{-q}$, in the range $10^3 \leq E_\gamma/m_e c^2 \leq 10^8$, and with $q = 1.8$ (Abdo et al. 2010). In addition, we use the *nominal* model of Aharonian (2001) for the EBL in the range from 0.1 to 1000 μm . For the cosmic background radiations beyond 0.1 μm we used data from Hauser et al. (2001). Contrary to Elyiv et al. (2009) we did not consider the deflection of e^+e^- pairs in the extragalactic magnetic field as well as the inverse Compton interactions with CMB photons. Here we took into account pair distributions resulting from just the first double photon collisions. Energy distribution and cross section of the relevant reactions were taken from (Aharonian 2003).

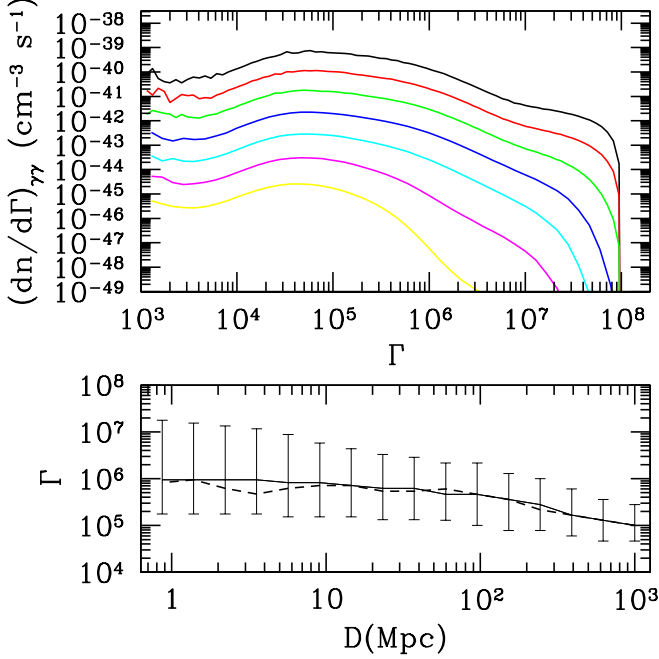


FIG. 1.— *Top*: Energy distribution of the beam pairs generated at distances, from top to bottom, of 3.5 (black), 9.1 (red), 23.3 (green), 60 (blue), 153 (cyan), 390 (magenta), and 1000 (yellow) Mpc from a blazar with equivalent isotropic gamma-ray luminosity of 10^{45} erg s $^{-1}$. *Bottom*: Peak (dash) and mean (solid) pair beam energy as a function of distance from the blazar, for an equivalent isotropic gamma-ray luminosity of 10^{45} erg s $^{-1}$. Vertical bars correspond to 68% percentile of the energy spread about the median.

Given the primary gamma-ray photon spectrum, we generated random gamma-photon interaction events. These are characterized by the random distance from the blazar at which the double photon collision occurs based on the EBL dependent mean free path of the high energy photons. Next we randomly generated the energies E_{\pm} of the produced $e^{+}e^{-}$ pairs, and evaluated the proper angle θ between each pair and the direction of the incident gamma-ray photon. For these quantities we used the analytical expressions for $\mu_e = \cos(\theta)$ in Schlickeiser et al. (2012).

The results of the calculation are shown in Fig. 1, for a blazar with equivalent isotropic gamma-ray luminosity of 10^{45} erg s $^{-1}$. The top panel shows the spectral energy distribution of the production rate of the pairs at several distances from the blazar, ranging from 3.5 Mpc (top, black line), to a 1 Gpc (bottom, yellow line). The bottom panel shows the peak (dash) and mean (solid) energy of the generated pairs, in units of $m_e c^2$, as a function of distance from the blazar. The Lorentz factor of the pairs is a monotonically decreasing function of distance, in the range $\Gamma=10^5 - 10^6$ up to a Gpc away from the blazar. This shows that pair production typically peaks at near infrared ($E_{\text{EBL}} \simeq 0.1$ eV) EBL target photons interacting with gamma-rays with energy $E_{\gamma} \sim (0.1-1)$ TeV. The vertical bars indicate the energy range encompassing 68% of the particles. In fact, there is considerable energy spread about the mean value, which decreases towards larger distances as the energy range of gamma-ray photons interacting with the EBL is also reduced. However, the beam particles remain always ultra-relativistic, a detail

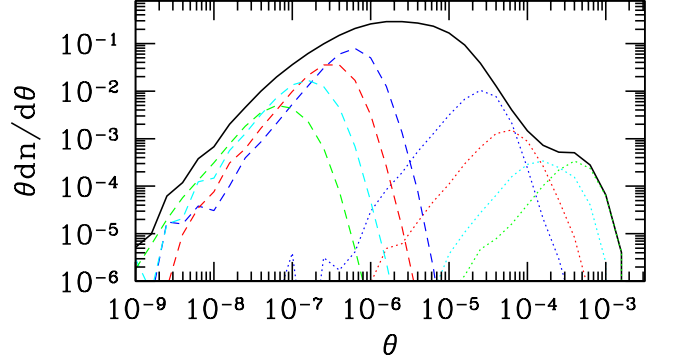


FIG. 2.— Angular distribution of beam pairs generated at 244 Mpc (solid), from the blazar. The colored curves indicate the contribution to the angular distribution from pairs in the energy range: $10^3-2.1 \times 10^3$ (dot green), $2.1 \times 10^3-4.6 \times 10^3$ (dot cyan), $4.6 \times 10^3-10^4$ (dot red), $10^4-2.15 \times 10^4$ (dot blue), which dominate the large angle end, and $10^6-2.1 \times 10^6$ (dash blue), $2.1 \times 10^6-4.6 \times 10^7$ (dash red), $4.6 \times 10^7-10^8$ (dash cyan), $10^8-2.15 \times 10^8$ (dash green) which dominate the small angle end.

relevant in the analysis below.

Fig. 2 shows the angular distribution of beam pairs at distances of 244 Mpc (black dash) from the blazar. The beam angular spread is of order $\Delta\theta \simeq 10^{-5}$, consistent with Eq. (5) and the value of Γ estimated above. The colored (dash and dot) curves show the angular distribution of pairs in eight different energy bins, indicating that the beam angular spread is primarily determined by pairs with $\Gamma \sim 10^4-10^6$.

The distribution that we use for the analysis of the pair beam stability below is the steady state one, obtained by balancing the production rate given in Fig. 1 with inverse Compton losses, i.e.

$$f(\Gamma) = \int_0^{\Gamma} \frac{\tau_{IC}(\varepsilon)}{\varepsilon} \left(\frac{dn(\varepsilon)}{d\varepsilon} \right)_{\gamma\gamma} d\varepsilon \quad (6)$$

where $\tau_{IC}(\Gamma) = \ell_{IC}/c$ is the energy dependent time scale for inverse Compton losses.

In Table 1, we report as a function of distant, D , from the blazar, the main properties of the beam, which are relevant to the analysis below. These include, the number density of the beam pairs, n_b ; the mean value of the inverse of the pairs Lorentz factor, $\langle \Gamma^{-1} \rangle^{-1}$, which enters the estimate of the max growth rate of the instability; the mean value of the pairs Lorentz factor, $\langle \Gamma \rangle$, which determines the mean energy of the beam; the mean square value of the pairs Lorentz factor divided by the mean value of the same, $\langle \Gamma^2 \rangle / \langle \Gamma \rangle$, which enters the estimate of the inverse Compton timescale; and the rms of the opening angle of the pairs, $\Delta\theta$, which also enters the growth rate of the instability. These Lorentz gamma factors differ considerably, and they all monotonically decrease with distance as in the bottom panel of Fig. 1.

Although the results in this and the next sections assume a blazar equivalent isotropic gamma-ray luminosity of 10^{45} erg s $^{-1}$. they can be generalized to other luminosities by rescaling the pair beam number density according to $n_b \rightarrow n_b(E_{\gamma} L_{\gamma} / 10^{45} \text{ erg s}^{-1})$.

2.3. IGM in Voids

TABLE 1
BEAM BASIC PROPERTIES FROM MONTE CARLO MODEL

D (Mpc)	n_b cm^{-3}	$\langle \Gamma^{-1} \rangle^{-1}$ (10^4)	$\langle \Gamma \rangle$ (10^5)	$\langle \Gamma^2 \rangle / \langle \Gamma \rangle$ (10^6)	$\Delta\theta$ (10^{-5})
0.87	2.81e-18	1.52	1.56	5.65	6.43
1.39	1.17e-18	1.28	1.53	5.50	8.30
2.22	4.73e-19	1.48	1.52	5.13	6.06
3.55	1.79e-19	1.39	1.48	4.65	6.32
5.68	7.48e-20	1.32	1.39	4.01	7.07
9.09	2.93e-20	1.33	1.35	3.28	7.60
14.55	1.14e-20	1.35	1.28	2.55	7.75
23.28	4.48e-21	1.28	1.20	1.94	7.50
37.25	1.65e-21	1.30	1.13	1.50	7.29
59.60	5.25e-22	1.44	1.11	1.26	8.76
95.37	1.86e-22	1.39	1.00	0.99	9.14
152.59	6.31e-23	1.34	0.86	0.75	8.88
244.14	2.03e-23	1.27	0.72	0.52	9.67
390.63	6.13e-24	1.19	0.58	0.32	11.0
625.00	1.75e-24	1.12	0.47	0.18	11.0
1000.00	4.71e-25	1.04	0.39	0.12	11.8

The analysis of the pair beam instability depends also on the thermodynamic properties of the plasma in cosmic voids, namely the number density of free electrons and their temperature. The number density of free electrons can be expressed as $n_v \simeq 2 \times 10^{-7} (1 + \delta)(1 + z)^3 \text{ cm}^{-3}$. The typical overdensity δ is taken to be the value at which the cumulative distribution of the IGM gas is 0.5. Using the simulations results presented in Sec. 4.2, and in particular the insets in Fig. 9, we estimate as representative value for the voids $\delta_v = -0.9(1 + z)$, where the redshift dependence is approximate but sufficient for our purposes. Note that this implies a redshift evolution of the bulk IGM density in voids $n_v \propto (1 + z)^4$. As for the gas temperature we assume $T_v \simeq \text{a few} \times 10^3 \text{ K} (1 + z)^{1.5}$, which reproduces the IGM temperature at mean density of a few $\times 10^4$ at redshift 3. This redshift dependence, while again a rough approximation, is acceptable for our purposes.

3. BEAM INSTABILITY: REACTIVE VS KINETIC

The blazar induced pair beam is subject to microscopic instabilities, in particular two-stream like instabilities, of both electrostatic and electromagnetic nature. The beam is neutrally charged, so no return current is induced. In the following we assume a sufficiently weak magnetic field, such that $\omega_H \ll \omega_p$, where ω_H is the cyclotron frequency, $\omega_p = (4\pi n_b e^2 / m_e)^{1/2}$ the plasma frequency of the IGM in voids and e the electron's charge. In this case, the instability is predominantly associated to Cherenkov emission of Langmuir waves, which operates under the resonant condition

$$\omega - \mathbf{k} \cdot \mathbf{v} = 0, \quad (7)$$

where \mathbf{k} is the wave-vector of the perturbation mode and \mathbf{v} the beam particles velocity. The pair particles contribute equally to the dielectric function, as they have the same mass, number density, velocity distribution, and plasma frequency, $\omega_{p,b} = (4\pi n_b e^2 / m_e)^{1/2}$. After separating the contributions from the background plasma and the beam particles, the dispersion relation for Langmuir waves, valid in the relativistic case, can be written as (Breizman 1990)

$$1 - \frac{\omega_p^2}{\omega^2} - \frac{4\pi e^2}{k^2} \int \frac{\mathbf{k} \cdot \partial f / \partial \mathbf{p}}{\mathbf{k} \cdot \mathbf{v} - \omega} d\mathbf{p} = 0, \quad (8)$$

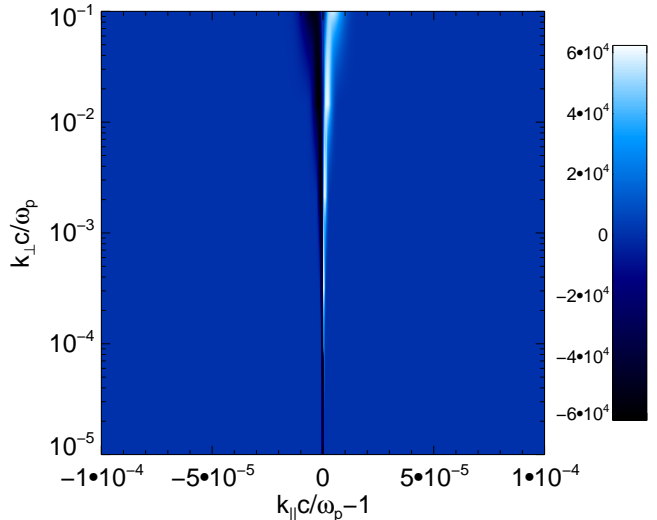


FIG. 3.— Normalized growth rate, $\gamma_k / \pi \omega_p (n_b / n_v)$, from Eq. (12) in the plane $k_{\parallel} c / \omega_p - k_{\perp} c / \omega_p$. Bright is positive, dark is negative and the uniformly colored region is zero, as it lies outside the resonant region.

where, $f(\mathbf{p})$, is the distribution function of the beam particles. There are two important regimes that characterize the unstable behavior of the beam, namely reactive and kinetic. In the reactive case, the beam's velocity spread, $\Delta \mathbf{v}$, is negligible so all particles can participate to the unstable behavior and the growth rate of the instability is therefore fastest. In the kinetic regime, on the other hand, the velocity spread is considerable and only the resonant particles contribute to the growth of Langmuir waves, so the growth rate is slower than in the reactive case. Formally, the reactive regime is applicable when (Breizman & Ryutov 1971)

$$|\mathbf{k} \cdot \Delta \mathbf{v}| \ll \gamma_r, \quad (9)$$

where γ_r is the reactive growth rate. In this case, the integral in Eq. (8) can be solve in a simplified way, which involves neglect of the velocity spread around the mean value. This leads to the estimate of the reactive growth rate which, maximized along the longitudinal component of the wave-vector reads (Fainberg et al. 1970)

$$\gamma_r \simeq \omega_p \left(\frac{n_b}{\Gamma n_v} \right)^{\frac{1}{3}} \left(\frac{k_{\parallel}^2}{k^2 \Gamma^2} + \frac{k_{\perp}^2}{k^2} \right)^{\frac{1}{3}}, \quad (10)$$

with $k_{\parallel} = \omega_p / v$, and k_{\parallel} , k_{\perp} the components of the wave-vector parallel and perpendicular to the beam direction, respectively. It is well known that, for an ultra-relativistic beam ($\Gamma \gg 1$), the fastest growing modes in the reactive regime are those quasi-perpendicular to the beam. This is due to the large suppression caused by relativistic inertia along the longitudinal direction (Fainberg et al. 1970). However, as shown later, for quasi-perpendicular directions of the wave vector, the reactive regime is not applicable.

When the approximation (9) is not valid, the growth rate is evaluated from a pole of the integrand in the dis-

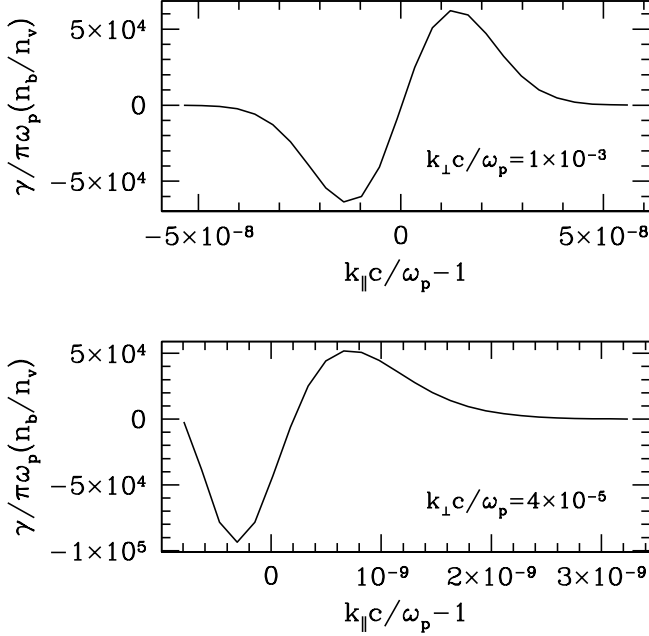


FIG. 4.— Normalized growth rate as a function of $k_{\parallel}c/\omega_p$ inside the the resonant region, for values of k_{\perp} where γ_k reaches its maximum values.

persion relation (8), namely

$$\gamma_k = \omega_p \frac{2\pi e^2}{k^2} \int \mathbf{k} \cdot \frac{\partial f}{\partial \mathbf{p}} \delta(\omega_p - \mathbf{k} \cdot \mathbf{v}) d\mathbf{p}. \quad (11)$$

If, as is the case here, despite the energy spread the particles remain ultra-relativistic and, $|\mathbf{v}| = c$, can be assumed, the above integral can be simplified to (Breizman & Mirnov 1970)

$$\gamma_k = -\omega_p \pi \frac{n_b}{n} \left(\frac{\omega_p}{kc}\right)^3 \int_{\mu_-}^{\mu_+} d\mu \frac{2g + (\mu - \frac{k_{\parallel}c}{\omega_p}) \frac{\partial g}{\partial \mu}}{[(\mu_+ - \mu)(\mu - \mu_-)]^{\frac{1}{2}}}, \quad (12)$$

where the integration variable μ is the angle between the particles and the beam direction, and

$$\mu_{\pm} = (\omega_p/kc)(k_{\parallel}/k \pm k_{\perp}/k \sqrt{k^2c^2/\omega_p^2 - 1}), \quad (13)$$

$$g(\theta) = \frac{m_e c}{n_b} \int p f(p, \theta) dp \simeq \langle \Gamma^{-1} \rangle \frac{1}{\Delta\theta^2} e^{-\frac{\theta^2}{\Delta\theta^2}}. \quad (14)$$

The second equality for $g(\theta)$ in Eq. (14) is found to be a good approximation based on results of the Monte Carlo model of the cascade. The integral for the growth rate in Eq. (12) can be evaluated numerically. The *qualitative* behavior of the growth rate, γ_k , on the plane $k_{\parallel} - k_{\perp}$ is summarized in Fig. 3 (Breizman & Ryutov 1971) for a beam at a Gpc from the blazar. Outside the narrow resonant region of k -space, corresponding in the plot to the uniform color, the growth rate is effectively null. In the narrow resonant region around $k_{\parallel} = \omega_p/c$, the growth can be positive (bright), negative (dark) and null, and for large enough values of k_{\perp} , it carries the sign of, $\omega_p/k_{\parallel} - c$ (see below). Within the resonant region, the growth rate as a function of k_{\parallel} has typically two extrema, a maximum and a minimum. This is shown in Fig. 4 for values of k_{\perp} of interest, i.e. where γ_k reaches its maximum values.

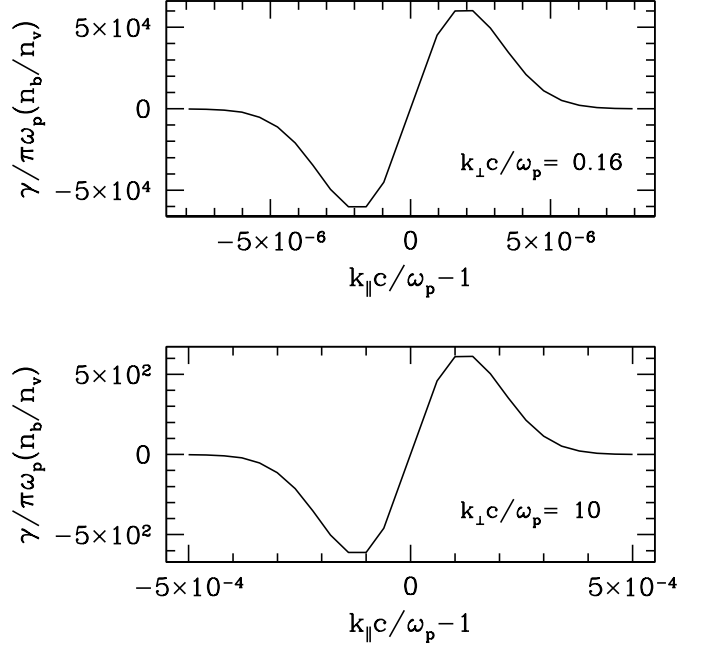


FIG. 5.— Normalized growth rate as a function of $k_{\parallel}c/\omega_p$ inside the the resonant region, for large values of k_{\perp} where γ_k starts to drop compared to its maximum value.

The growth rate has its largest values where $k_{\perp}c/\omega_p \lesssim 1$, and decays rapidly in the opposite limit. This can be seen from Fig. 5 where γ_k is plotted for values of k_{\perp} close to and much larger than ω_p/c (cf. scale of y-axis). Finally, we find that the growth rate, maximized with respect to k_{\parallel} and as a function of k_{\perp} , can be well approximated by the following expression by Breizman & Ryutov (1971)

$$\gamma_k \simeq \omega_p \langle \Gamma^{-1} \rangle \frac{n_b}{n_v} \frac{1}{\Delta\theta^2} \frac{\omega_p^2}{\omega_p^2 + k_{\perp}^2 c^2}, \quad (15)$$

which we will be using in the following.

3.1. Fastest Growing Modes vs Coulomb Collisions

For particles of an ultra-relativistic beam with modest angular spread, $\Delta\theta \ll 1$, we can assume $v_{\parallel} \simeq c$ and $v_{\perp} \simeq c\Delta\theta$. If the energy spread, $\Delta E/E \lesssim 1$, then the longitudinal velocity spread of the beam is

$$\Delta v_{\parallel} \simeq c \frac{\Delta E}{\langle \Gamma \rangle^2 E} + c\Delta\theta^2. \quad (16)$$

Thus, for the angular spread and Lorentz factor characteristic of the blazars induced beam, the longitudinal velocity spread is negligible with respect to the perpendicular velocity spread. It turns out that, the first and second terms in Eq. (16) are comparable to within a factor of a few, so for the sake of simplicity in the following we retain the second term only, neglecting any fudge factor. If we then use Eq. (9) and (16), with the estimates for the beam angular spread and bulk Lorentz factor from the previous Section, we find that virtually all modes require a kinetic description, unless

$$\frac{k_{\perp}}{k} \lesssim \times 10^{-5} \left(\frac{n_b/n_v}{10^{-15}}\right) \left(\frac{\langle \Gamma \rangle}{10^5}\right)^{-1} \left(\frac{\Delta\theta}{10^{-5}}\right)^{-3}. \quad (17)$$

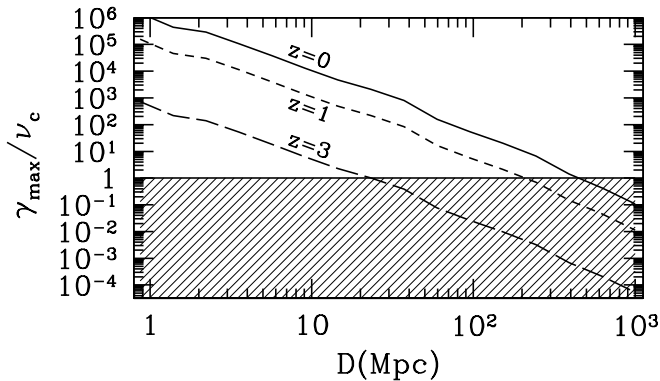


FIG. 6.— Ratio of instability max growth rate, γ_{max} , to Coulomb collision rate, ν_c , for redshift $z=0$ (solid), $z=1$ (short dash) and $z=3$ (long dash). The shaded area corresponds to the absolutely stable region where $\gamma_{max} \leq \nu_c$.

The max growth rate occurs at k_{\perp} provided by the above estimate. For smaller values we enter the reactive regimes and relativistic inertia increases. For larger values we are in the kinetic regime where the growth rate decreases due to the increasing velocity spread along \mathbf{k} , although the decrease becomes significant only for $k_{\perp} \geq \omega_p/c$. The fastest growth rate for modes with $k_{\perp} \leq \omega_p/c$ is therefore given by

$$\gamma_{max} \simeq \omega_p \langle \Gamma^{-1} \rangle \frac{n_b}{n_v} \frac{1}{\Delta\theta^2} = 4 \times 10^{-12} \text{s}^{-1} \times \left(\frac{n_v}{2 \times 10^{-8} \text{cm}^{-3}} \right)^{-\frac{1}{2}} \left(\frac{\langle \Gamma^{-1} \rangle}{10^{-4}} \right)^{-1} \left(\frac{\Delta\theta}{10^{-4}} \right)^{-2} \left(\frac{D}{\text{Gpc}} \right)^{-2}, \quad (18)$$

where we have taken $n_b \simeq 10^{-24} \text{cm}^{-3}$ at a Gpc from a blazar of luminosity $E_{\gamma} L_{\gamma} = 10^{45} \text{erg s}^{-1}$. A basic condition for the growth of an instability is that its growth rate exceeds the collisional damping rate, i.e. $\gamma_{max} \gg \nu_c$, where (Huba 2009)

$$\nu_c \simeq 10^{-11} \text{s}^{-1} \left(\frac{n_v}{2 \times 10^{-8} \text{cm}^{-3}} \right) \left(\frac{T_v}{3 \times 10^3 \text{K}} \right)^{-\frac{3}{2}}, \quad (19)$$

and for the Coulomb logarithm we have used $\Lambda_c = 27.4$ (Huba 2009). In Fig. 6, we plot the ratio γ_{max}/ν_c as a function of distance from the blazar, using the values reported in Table 1, which again apply for a blazar of equivalent isotropic gamma-ray luminosity of $10^{45} \text{erg s}^{-1}$. The solid, dash and long-dash curves correspond to redshift $z=0$, $z=1$ and $z=3$, respectively. The redshift dependence is obtained by using the void average density and temperature redshift dependences discussed in Sec. 2.3, together with the redshift dependence of n_b given in Sec. 2.1. The shaded area corresponds to the region where the instability is inhibited by collisions. The plot shows that the instability can only develop at distances of less than a 50 Mpc at redshift $z=0$ and about 20 physical Mpc $z=3$.

4. BEAM STABILIZATION

As shown in the previous section, pair beams within a certain distance of the parent blazar may be unstable due to the excitation of Langmuir waves. In this section we further analyse these unstable conditions. In particular we consider nonlinear effects on plasma waves due to

scattering off thermal ions and density inhomogeneities. We begin, however, with a brief outline of the main features of the relaxation process (for a detailed description see, e.g., Melrose 1989; Breizman & Ryutov 1974). An important assumption in what follows is that the level of plasma turbulence remains low compared to the plasma thermal energy, so that a perturbative approach is valid. This, will be verified at the end of the analysis.

The presence of excited plasma waves causes the beam particles to diffuse in momentum space. This continues until the particle momentum distribution has flattened, and Cherenkov emission ($\propto \partial f / \partial p$) is suppressed. According to the calculations of Grognard (1975), this process of quasilinear relaxation takes about 50-100 instability growth timescales to complete. In general, however, other processes occur that reduce the energy of resonant waves the particles interact with, thus stabilising the beam. Spatial transport effects may contribute in two ways. On the one hand, waves drift along the energy density gradient at the group velocity, $v_g \simeq 3v_i^2/c$. For the case of interest here, this process is negligible, due to the smallness of the group velocity and spatial gradients of the wave energy. In addition, however, if the plasma frequency is not constant in space due to plasma inhomogeneities, the wave-vector will change in time, destroying the particle-wave resonant conditions. This effect turns out to be important and will be considered further below.

In the limit of weak turbulence, second order effects can also play an important role (Melrose 1989; Breizman & Ryutov 1974). In short, these are described in terms of three-wave interactions and particle-wave scattering. Three waves interactions involve, in addition to Langmuir waves, at least one electromagnetic wave, because the frequency resonance condition cannot be fulfilled with three Langmuir waves alone. Compared to other processes discussed below, however, they are of order $k_B T / m_e c^2$, so they turn out to be negligible for the conditions of interest here. As for particle-wave scattering, Langmuir waves can undergo induced scattering either by electrons or ions, into either Langmuir waves or electromagnetic waves. The latter process is suppressed in presence of inhomogeneities, so it will be neglected in the following. Furthermore, as we are considering waves with wavelength larger than the Debye length, the scattering by thermal ions is considerably more important than thermal electrons. This is because for thermal ions only, the superposed effects of the bare and shielding charge (basically an electron of opposite charge as the bare charge) do not cancel out, due to the much larger mass of the ion compared to the electron. Therefore, with regard to second order nonlinear effects in the following we only consider induced scattering off thermal ions.

4.1. Nonlinear Landau damping

In this section we consider in some detail the main process that we believe compensates the growth of Langmuir waves, i.e. induced scattering off plasma ions, also known as non-linear Landau damping (Tsytovich & Shapiro 1965; Breizman et al. 1971; Lesch & Schlickeiser 1987). In this process, a thermal ion, with characteristic velocity, v_{ti} , interacts with the beat wave produced by two

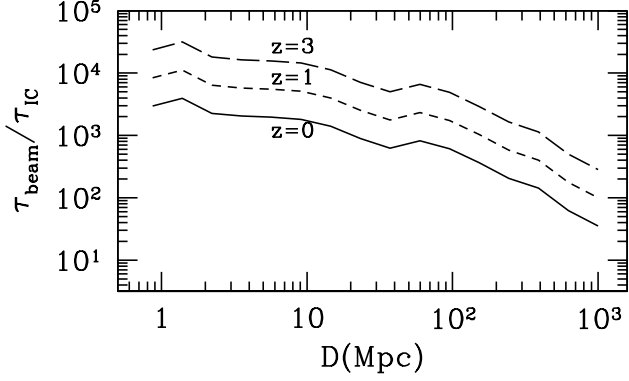


FIG. 7.— Ratio of beam relaxation timescale, τ_{beam} , to inverse Compton loss time, τ_{IC} , for redshift $z=0$ (solid), $z=1$ (short dash) and $z=3$ (long dash).

Langmuir oscillations, $\omega(\vec{k})$, $\omega(\vec{k}')$, under the condition for Cherenkov interaction, i.e.

$$\omega(\mathbf{k}) - \omega(\mathbf{k}') = (\mathbf{k} - \mathbf{k}') \cdot \mathbf{v}_{ti}. \quad (20)$$

The rate of induced scattering of Langmuir waves off thermal ions in a Maxwellian plasma with number density n and ion/electron temperature T_i/T_e respectively, is (e.g., Melrose 1989)

$$\begin{aligned} \gamma_{nl}(\mathbf{k}) &= \frac{3(2\pi)^{\frac{1}{2}}}{2} \frac{T_i T_e}{(T_i + T_e)^2} \int \frac{d^3 \mathbf{k}'}{(2\pi)^3} \frac{\hat{W}(k')}{nm_e v_{ti}} \quad (21) \\ &\times \left(\frac{\mathbf{k} \cdot \mathbf{k}'}{kk'} \right)^2 \frac{k'^2 - k^2}{|\mathbf{k}' - \mathbf{k}|} \exp \left[-\frac{1}{2} \left(\frac{3}{2} \frac{v_{te}^2}{\omega_p v_{ti}} \frac{k'^2 - k^2}{|\mathbf{k}' - \mathbf{k}|} \right)^2 \right], \end{aligned}$$

where $\hat{W}(k)$ indicates the spectral energy density of Langmuir waves. The growth rate, $\gamma_{nl}(\mathbf{k})$, bears the sign of $(k' - k)$. This indicates that as a result of induced scattering, Langmuir waves cascade towards regions of phase space of lower wave-vectors, i.e. lower energies, the energy difference being absorbed by the thermal ions. Eventually, the wave energy is transferred to modes with wavenumber, k , small enough that the wave phase-speed, $\omega/k > c$, exceeds the speed of light, and resonance with the beam particles is lost. The wavenumbers allowed in the scattering process are constrained by the integral expression in Eq. (21). In particular, the following condition must be fulfilled:

$$\frac{|k'^2 - k^2|}{|\mathbf{k}' - \mathbf{k}|} \leq \omega_p \frac{v_{ti}}{v_{te}^2} \simeq 35 \times \frac{\omega_p}{c} \left(\frac{T_v}{3 \times 10^3 \text{K}} \right)^{-\frac{1}{2}}. \quad (22)$$

The above constrain is satisfied for the case of differential scattering, i.e. $\Delta k/k \ll 1$, whereby $k \sim k'$ and $\mathbf{k}' \sim -\mathbf{k}$. In this case Langmuir waves, generated with wavenumber, $k \sim \omega_p/c$, parallel to the beam, are isotropized. This reduces the level of resonant energy density by a factor $\sim \Delta\theta^2/4\pi$, increasing somewhat the lifetime of the beam. However, given the low temperature of the IGM in voids, the more efficient integral scattering, with $k' \ll k$, is also allowed. In this case Langmuir waves are mostly kicked out of resonance in a single scattering event, reducing dramatically the level of resonant energy density and suppressing the instability.

The general solution for the evolution of the energy density in plasma waves is a non trivial task, as it re-

quires solving for integro-differential equations that describe the detailed energy transfer of the wave energy across different modes. However, for a conservative estimate, we can neglect differential scattering, and evaluate the rate of induced integral scattering from Eq. (21) using the condition $k' \ll k$. We thus obtain

$$\gamma_{nl} \simeq \omega_p \frac{W_{nr}}{n_v k_B T_v} \frac{v_{te}^2}{v_{ti} c} \quad (23)$$

where W_{nr} is the total energy density in Langmuir waves at $k \ll \omega_p/c$, i.e. non-resonant with the beam. This energy density is excited by the non-linear scattering process and for the most part is dissipated by Coulomb collisions at a rate ν_c (see further discussion below). Thus it evolves according to

$$\frac{\partial W_{nr}}{\partial t} = 2\tilde{\gamma}_{nl} W_{nr} W_r - \nu_c W_{nr}, \quad (24)$$

where we have used, $\tilde{\gamma}_{nl} \equiv \gamma_{nl}/W_{nr} = \omega_p(1/n_v k_B T_v)(v_{te}^2/v_{ti} c)$ and W_r is the total energy density in Langmuir waves at $k \sim \omega_p/c$, i.e. resonant with the beam. The latter obviously evolves according to

$$\frac{\partial W_r}{\partial t} = 2\gamma_{max} W_r - 2\tilde{\gamma}_{nl} W_{nr} W_r, \quad (25)$$

where we have neglected the role of collisions (i.e. we assume, $\gamma_{max} \gg \nu_c$, as required for the existence of the instability). Eq. (25) and (24) form a well-known Lotka-Volterra system of coupled non-linear differential equations, which has stable periodic solutions, with the following average values for the energy densities:

$$\overline{W}_{nr} = \frac{\gamma_{max}}{\tilde{\gamma}_{nl}}, \quad \overline{W}_r = \frac{\nu_c}{2\tilde{\gamma}_{nl}}. \quad (26)$$

In this regime, the transfer rate of Langmuir waves out of resonance by non-linear Landau damping equals on average their production rate, i.e. $\gamma_{nl} \simeq \gamma_{max}$. Thus, the beam emission of Langmuir waves is only linear in time, with an average power $P(W_r) = 2\tilde{\gamma}_{max} W_r$, and the beam relaxation timescale at redshift $z = 0$ is:

$$\begin{aligned} \tau_{beam} &\simeq \frac{n_b \langle \Gamma \rangle m_e c^2}{2\gamma_{max} \overline{W}_r} = 1.5 \times 10^9 \text{yr} \left(\frac{n_v}{2 \times 10^{-8} \text{cm}^{-3}} \right)^{-1} \\ &\times \left(\frac{\langle \Gamma^{-1} \rangle}{10^{-4}} \right) \left(\frac{\langle \Gamma \rangle}{10^5} \right) \left(\frac{\Delta\theta}{10^{-4}} \right)^2 \left(\frac{T_v}{3 \times 10^3 \text{K}} \right). \quad (27) \end{aligned}$$

The above timescale should be compared with the pairs cooling time on the Cosmic Microwave Background, $\tau_{IC} = \ell_{IC}/c \simeq 3 \times 10^6 (E_{\pm}/\text{TeV})^{-1} (1+z)^{-4}$ yr. The ratio of these timescales is plotted in Fig. 7 using the values reported in Table 1, as a function of distance from our reference blazar with isotropic gamma-ray luminosity of 10^{45} erg s $^{-1}$. At redshift $z = 0$ (solid line) the beam appears to be stable on significantly longer timescales than the inverse Compton emission energy loss timescale, particularly within 100 Mpc from the blazar, where the average value of Γ of the pairs tends to be higher. This conclusion is reinforced at higher redshifts (dash line for $z = 3$), where the redshift dependence is inferred as in Sec. 3.1.

The above analysis works in the weak turbulence regimes, which requires that the energy density of resonant Langmuir waves be a small fraction of the beam

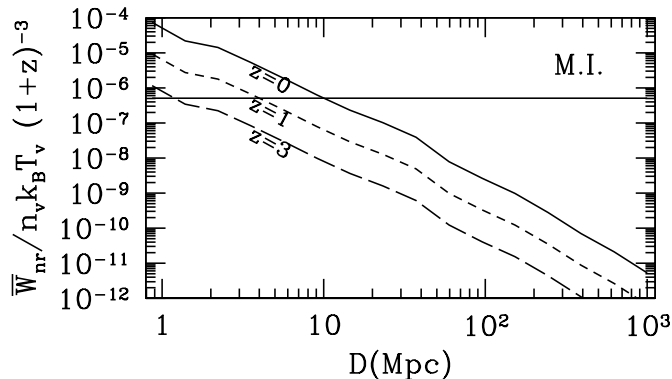


FIG. 8.— Ratio of nonresonant waves to thermal energy as a function of distance from our reference blazar, for redshift $z=0$ (solid), $z=1$ (short dash) and $z=3$ (long dash). The horizontal line correspond to the threshold for the onset of the modulation instability.

energy density. For the typical values of IGM gas and beam parameters used above this requirement is readily fulfilled as, $\bar{W}_{nr}/n_b \Gamma m_e c^2 \simeq 3 \times 10^{-6}$, warranting our approach limited to second order processes.

Another consistency check to be performed concerns the assumption of collisional dissipation of the long wavelength Langmuir waves. In fact, accumulation of energy in these non-resonant waves can generate modulation instability of the background plasma if (Breizman 1990),

$$\frac{\bar{W}_{nr}}{n_v k_B T_v} \geq k^2 \lambda_D^2 \sim k_B T_v / mc^2. \quad (28)$$

In Fig. 8 the ratio on the LHS of the above equation is plotted as a function of distance from our reference blazar using the values in Tab. 1. The solid line corresponds to redshift $z = 0$ and the horizontal line is the nominal threshold value for the onset of the modulation instability. For redshifts higher than $z = 0$, we plot for comparison with the same threshold line the same ratio on the LHS of Eq. (28) but divided by a factor $(1+z)^3$ to account for the IGM temperature redshift dependence (see Sec. 2.3).

The plot shows that the assumption of collisional dissipation of the long wavelength Langmuir waves is always valid except at short distances from low redshift blazars. The modulation instability deserves more attention than the scope of the current paper can afford. Here we notice that, while the modulation instability could stabilize the beam (Nishikawa & Ryutov 1976), it could also provide an effective dissipation rate that is more efficient than collisions. In this case the level of energy density of resonant waves, W_r , will increase with consequent reduction of the beam lifetime (see Eq. 26-4.1). However, because the threshold condition for triggering the modulation instability depends quadratically on the temperature (see Eq. 28), should the background plasma suffers even modest heating caused by the beam relaxation, the modulation instability will quickly stabilize (at below the Mpc scale), restoring the conditions for collisional dissipation of the nonresonant waves.

Therefore, in conclusion, from the above analysis together with the findings in in Sec. 3.1 it appears that the beam is stable at basically all relevant distances from the blazar. As a result, the beam instability plays only a

secondary role on the electromagnetic shower, the beam dynamics and the thermal history of the IGM.

4.2. Plasma Inhomogeneities

In addition to the kinetic effects described above, the energy density of the plasma waves evolves in time due to spatial gradients effects according to

$$\frac{d}{dt} \hat{W}(x, t, k) = \frac{\partial \hat{W}}{\partial t} + \mathbf{v}_g \nabla_{\mathbf{x}} \hat{W} - \nabla_{\mathbf{x}} \omega \cdot \nabla_{\mathbf{k}} \hat{W}, \quad (29)$$

where for the rate of change of the wave-vector we have used the equation of geometric optics

$$\frac{d\mathbf{k}}{dt} = -\nabla_{\mathbf{x}} \omega. \quad (30)$$

The first and second terms on the RHS of (29) describe as usual explicit time dependence and the effects of spatial gradients discussed at the beginning of Sec. 4. The last term describes the change in \hat{W} associated with modifications of the waves wave-vector as a result of inhomogeneities. This term is important because, just like induced scattering by thermal ions, it transfers the excited Langmuir waves to wavemodes that are out of resonance with the beam particles, therefore suppressing the instability (Breizman & Ryutov 1971; Nishikawa & Ryutov 1976).

For Langmuir waves the most important contribution to, $\nabla_{\mathbf{x}} \omega$, comes from density inhomogeneities. In addition, the beam stabilization mainly results from changes in the longitudinal component of the wave vector. Therefore, we restrict our analysis to this case only, and write

$$\frac{dk_{\parallel}}{dt} \simeq \frac{1}{2} \frac{\omega_p}{\lambda_{\parallel}}, \quad (31)$$

with $\lambda_{\parallel} = n_v / (\vec{\nabla} n_v)_{\parallel}$, the length scale of the density gradient along the beam.

In order to estimate the scale lengths of IGM density gradients, λ , we have carried out a cosmological simulation of structure formation including hydrodynamics, dark matter, and self-gravity as described in Miniati & Colella (2007). For the cosmological model we adopted a flat Λ CDM universe with the following parameters: total mass density, normalized to the critical value for closure, $\Omega_m = 0.2792$; normalized baryonic mass density, $\Omega_b = 0.0462$; normalized vacuum energy density, $\Omega_{\Lambda} = 1 - \Omega_m = 0.7208$; Hubble constant $H_0 = 70.1 \text{ km s}^{-1} \text{ Mpc}^{-1}$; spectral index of primordial perturbation, $n_s = 0.96$; and rms linear density fluctuation within a sphere of comoving radius of $8 h^{-1} \text{ Mpc}$, $\sigma_8 = 0.817$, where $h \equiv H_0/100$ (Komatsu et al. 2009). The computational box has a comoving size $L = 50 h^{-1} \text{ Mpc}$, is discretized with 512^3 comoving cells, corresponding to a nominal spatial resolution of $100 h^{-1} \text{ comoving kpc}$. The collisionless dark matter component is represented with 512^3 particles with mass $6 \times 10^3 h^{-1} M_{\odot}$.

Fig. 9 shows the range of scale lengths of IGM density gradients as a function of IGM gas over-density, for three different cosmological redshifts, $z = 0$ (top), $z = 1$ (middle) and $z = 3$ (bottom). Accordingly, the distance covered by the beam particles during the fastest growth time, $\sim c \gamma_{max}^{-1} \simeq 1 \text{ kpc}$, is much shorter than the typical

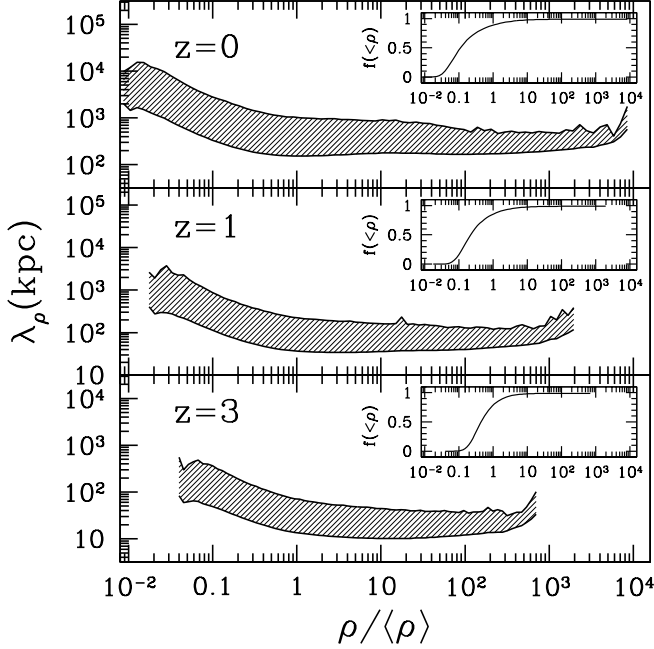


FIG. 9.— Characteristic length scale of density gradient in the IGM as a function of IGM gas over-density. The shaded area covers \pm one root-mean-squared value about the average. The inset shows the gas cumulative distribution as a function of over-density.

scale-length of density gradients. This corresponds to the case of regular, as opposed to random, inhomogeneities.

It is clear that in order for the excited waves to have an effect on the beam, the beam-waves interaction under resonant conditions must continue for a sufficiently long time. Therefore, the condition for wave excitation is expressed as (Breizman & Ryutov 1971)

$$\gamma_{max} \frac{\Delta k_{\parallel}}{|dk_{\parallel}/dt|} = \gamma_{max} \frac{2\lambda_{\parallel} \Delta k_{\parallel}}{\omega_p} > \Lambda_c, \quad (32)$$

where Λ_c is the Coulomb logarithm and Δk_{\parallel} the change in longitudinal component of the wave-vector allowed by the resonant condition (7). Using Eq. (7) (and neglecting the term $\Delta E/E\Gamma^2$) to obtain, $\Delta k_{\parallel} \lesssim \frac{\omega_p}{c} \Delta\theta^2 + k_{\perp} \Delta\theta$, Eq. (32) can be solved to express the condition for wave excitation in terms of λ_{\parallel} , i.e.

$$\lambda_{\parallel} \geq \frac{c}{2\omega_p} \langle \Gamma^{-1} \rangle \frac{n_v}{n_b} \Lambda_c \left(1 + \frac{k_{\perp}}{k_{\parallel} \Delta\theta} \right)^{-1} > 10^6 \text{ kpc} \\ \times \left(\frac{D}{\text{Gpc}} \right)^2 \left(\frac{\langle \Gamma^{-1} \rangle}{10^{-4}} \right) \left(\frac{\Delta\theta}{10^{-4}} \right) \left(\frac{\Lambda_c}{30} \right) (1+z)^2 \quad (33)$$

where in the second inequality we have used, $\kappa_{\perp} \simeq \kappa_{\parallel}$, which corresponds to the most favourable case for the instability growth in the presence of inhomogeneities, and again the redshift dependence is derived as described in Sec. 3.1. We can again plot the minimal values of λ_{\parallel} allowed for the growth of the beam instability using the parameter values for the beam from Table 1. This is shown by the oblique lines in Fig. 10, for redshift $z = 0$ (solid), $z = 1$ (dash) and $z = 3$ (long dash). The three horizontal thin lines (with the same line style as the oblique lines at the same redshift), correspond to the mean scale-length of density inhomogeneities at typical

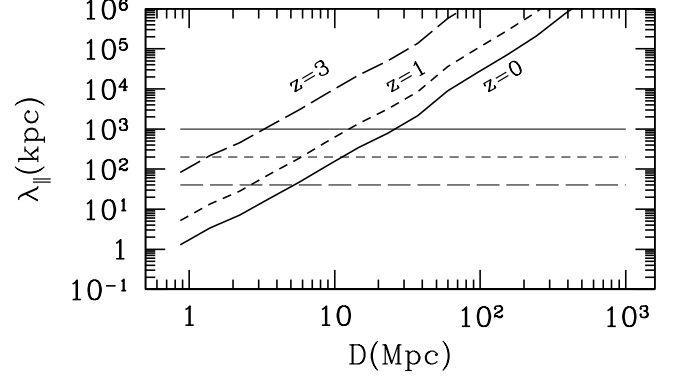


FIG. 10.— Oblique lines correspond to minimal values of λ_{\parallel} allowed for the growth of the beam instability as a function of distance from the blazar obtained using values in Table 1. Horizontal thin lines correspond to the mean scale-length of density inhomogeneities at typical void over-density (i.e., where the cumulative gas distribution function is 0.5), extracted from Fig. 9. Solid, dash and long dash correspond to redshift $z = 0$, $z = 1$, and $z = 3$.

void over-density (i.e., where the cumulative gas distribution function is 0.5), extracted from Fig. 9. The figure shows that the growth of Langmuir waves is severely constrained by the presence of inhomogeneities, except for regions close to the blazars, i.e. at distances $D < 30, 6, 1$ Mpc, for $z = 0, 1, 3$, respectively. Inhomogeneities provide another independent argument against the growth of Langmuir waves and the unstable behavior of the pair beam. While non-linear Landau damping weakens with distance from the blazar (see Fig. 6), the impact of inhomogeneities becomes stronger (see Fig. 10), so that the stabilization effects of the two processes compensate each other at different distances.

5. CONCLUSION

We considered the stability properties of a low density ultra relativistic pair beam produced in the intergalactic medium by multi-TeV gamma-ray photons from blazars. The physical properties of the pair beam are determined through a Monte Carlo model of the electromagnetic cascade. In summary we find that the combination of kinetic effects, non-linear Landau damping and density inhomogeneities appear to considerably stabilize blazars induced ultra-relativistic beams over the inverse Compton loss timescale, so that the electromagnetic cascade remains mostly unaffected by the beam instability. This implies that the lack of a bumpy feature at multi-GeV energies in the gamma-ray spectrum of distant blazars cannot be attributed such instabilities and can in principle be related to the presence of an intergalactic magnetic field. Finally, heating of the IGM by pair beams appears negligible.

F.M. acknowledges very useful discussions with B. N. Breizman and A. Benz, and comments from D. D. Ryutov, and R. Schlickeiser. We are grateful to D. Potter for making available the `grafic++` package for cosmological initial conditions. The numerical calculations were performed at the Swiss National Supercomputing Center.

REFERENCES

- Abdo, A., Ackermann, M., Ajello, M. 2010, *A&A*, 710, 1271-1285
- Ajello, M. and Shaw, M. S. and Romani, R. W. and Dermer, C. D. and Costamante, L. and King, O. G. and Max-Moerbeck, W. and Readhead, A. and Reimer, A. and Richards, J. L. and Stevenson, M. 2012, *ApJ*, 751, 108
- Aharonian, A. F., arXiv:astro-ph/0112314 (2001)
- Aharonian, A. F., 2003, *Very High Energy Cosmic Gamma Radiation*, World Scientific Publ., Singapore
- Aharonian, F. A. et al. 2006, *Nature*, 440, 1018
- Benz, A. 1993, *Plasma Astrophysics* (Kuwler: Dordrecht)
- Bertschinger, E. 2001, *ApJS*, 137, 1
- Bonometto, S., Rees, M. R. 1971, *MNRAS*, 152, 21
- Breizman, B. N. 1990, *Reviews of Plasma Physics*, 15, 61 (ed. B. Kadomstev)
- Breizman, B. N., Mirnov, V. V. 1970, *Geomagn. Aeron.*, 10, 34
- Breizman, B. N., Ryutov, D. D. 1971, *JETP*, 33, 220
- Breizman, B. N., Ryutov, D., Chebotaev, P. Z. 1972, *JETP*, 35, 72
- Breizman, B. N., Ryutov, D. D. 1974, *Nucl. Fusion*, 14, 873
- Broderick, A. E., Chang, P., Pfrommer, C. 2012, *ApJ*, 752, 22
- Chang, P., Broderick, A. E., Pfrommer, C. 2012, *ApJ*, 752, 23
- Dermer, C. D., Cavadini, M., Razzaque, S., Finke, J. D., Chiang, J., Lott, B. 2011, *ApJ*, 733, L21
- Dolag, K., Kachelriess, M., Ostapchenko, S., Tomàs, R. 2011, *ApJ*, 727, L4
- Elyiv, A., Neronov, A., D. V. Semikoz, D. V. 2009, *Phys. Rev. D*, 80, 023010
- Ensslin, T. A., Pfrommer, C., Miniati, F., Subramanian, K. 2011, *A&A*, 527, A99
- Fainberg, Ya. B., Shapiro, V. D., Shevchenko, V. I. 1970, *JETP*, 30, 528
- Franceschini, A., Rodighiero, G., Vaccari, M. 2008, *A&A*, 487, 837
- Gould, R. J. & Schröder, G. P. 1967, *Phys. Rev. Lett.*, 16, 252
- Grognard, R. J.-M. 1975, *Aust. J. Phys.*, 28, 731
- Hauser, M., Dwek, E. 2001, *A&A*, 39, 249-307
- Huba, J. D. 2004, *NRL Plasma Formulary*, (Washington DC: Naval Research Laboratory) NRL/PU/679009-523
- Kaplan, S. A., Tsytovich, V. N. 1973, *Plasma Astrophysics*, (Pergamon Press: Oxford)
- Kneiske, T. M., Bretz, T., Mannheim, K., Hartmann, D. H. 2004, *A&A*, 413, 807
- Komatsu, E., et al. 2009, *ApJS*, 180, 330
- Lesch, H., Schlickeiser, R. 1987, *A&A*, 179, 93
- Melrose, D. B. 1989, *Instabilities in Space and Laboratory Plasmas* (Cambridge University Press)
- Miniati, F., Bell, A. R., 2011, *ApJ*, 729, 73
- Miniati, F., & Colella, P. 2007, *Journal of Computational Physics*, 227, 400
- Murase, K., Takahashi, K., Inoue, S., Ichiki, K., Nagataki, S. 2008, *ApJ*, 686, L67
- Neronov, A., Semikoz, D. 2009, *Phys. Rev. D*, 80, 123012
- Neronov, A., Vovk, I. 2010, *Science*, 328, 7
- Neronov, A., Semikoz, D., Kachelriess, M., Ostapchenko, S., Elyiv, A. 2010, *ApJ*, 719, L130
- Nishikawa, K., Ryutov, D. D. 1976, *Journal of the Physical Society of Japan*, 41, 1757
- Peebles, P. J. E. 1993, *Principles of Physical Cosmology* (Princeton New Jersey: Princeton University Press)
- Pfrommer, C., Chang, P., Broderick, A. E. 2012, *ApJ*, 752, 24
- Plaga, R. 1995, *Nature*, 374, 430
- Rudakov, L. I. 1971, *JETP*, 32, 1134
- Schlickeiser, R., Elyiv, A., Ibscher, D., Miniati, F. 2012, *ApJ*, submitted
- Tavecchio, F., Ghisellini, G., Bonnoli, G., Foschini, L. 2011, *MNRAS*, 414, 3566
- Taylor, A. M., Vovk, I., Neronov, A. 2011, *A&A*, 529, A144
- Tsytovich, V. N., Shapiro, V. D. 1965, *Nuclear Fusion*, 5, 228